



Nanoscale Insight into the Degradation Mechanisms of the Cartilage Articulating Surface Preceding OA

Journal:	<i>Biomaterials Science</i>
Manuscript ID	BM-ART-03-2020-000496.R2
Article Type:	Paper
Date Submitted by the Author:	05-Jun-2020
Complete List of Authors:	Shoib, Tooba; University of Illinois at Urbana-Champaign Yuh, Catherine; Rush University Medical Center, Department of Orthopedic Surgery Wimmer, Markus; Rush University Medical Center, Department of Orthopedic Surgery Schmid, Thomas; Rush University Medical Center, Department of Orthopedic Surgery Espinosa-Marzal, Rosa; University of Illinois at Urbana-Champaign

ARTICLE

Nanoscale Insight into the Degradation Mechanisms of the Cartilage Articulating Surface Preceding OA

Received 00th January 20xx,
Accepted 00th January 20xx

Tooba Shoaib^{a,†}, Catherine Yuh^{b,†}, Markus A. Wimmer^{b,*}, Thomas Schmid^b, and Rosa M. Espinosa-Marzal^{a,c*}

DOI: 10.1039/x0xx00000x

Osteoarthritis (OA) is a degenerative joint disease and a leading cause of disability globally. In OA, the articulating surface of cartilage is compromised by fissures and cracks, and sometimes even worn away completely. Due to its avascular nature, articular cartilage has a poor self-healing ability, and therefore, understanding the mechanisms underlying degradation is key for OA prevention and for optimal design of replacements. In this work, the articulating surface of bovine cartilage was investigated in an environment with enhanced calcium concentration -as often found in cartilage in relation to OA- by combining atomic force microscopy, spectroscopy and an extended surface forces apparatus for the first time. The experimental results reveal that increased calcium concentration irreversibly weakens the cartilage's surface layer, and promotes stiction and high friction. The synergistic effect of calcium on altering the cartilage surface's structural, mechanical and frictional properties is proposed to compromise cartilage integrity at the onset of OA. Furthermore, two mechanisms at the molecular level based on the influence of calcium on lubricin and on the aggregation of the cartilage's matrix, respectively, are identified. The results of this work might not only help prevent OA but also help design better cartilage replacements.

Introduction

Articular cartilage (AC) is a load-bearing avascular tissue in synovial joints that provides low-friction motion between the articulating surfaces. The wear-resistant tissue is composed of an extracellular matrix (ECM) with a well-ordered three-dimensional structure, secreted by a small number of embedded chondrocytes cells, and ~70%-80% in weight of imbibed fluid. The primary components of the ECM are Type II collagen fibrils (~20%) and proteoglycans like aggrecan (~7%), with a graded distribution from the articular surface to the underlying bone. While collagen contributes predominantly to the shear and tensile strength of the cartilage, proteoglycans, with a high density of negative charge, draw water into the tissue and generate an osmotic swelling that is resisted by the collagen network, thereby yielding a hydrated tissue that resists compressive loads². Yet early studies recognized that an amorphous (gel-like) surface layer of several microns in thickness -also known as the *lamina splendens*^{3, 4}- covers the

cartilage's superficial zone. This surface layer has a distinct structure, high water content and is much softer than the underlying cartilage⁵. Its composition, however, is still under debate. Some works propose it is collagen-free, and rich in proteoglycans, hyaluronan, along with gel-forming mucins like lubricin, and phospholipids⁶; while other images reveal fine collagen fibrils, as well as a network of elastic fibers composed of elastin and fibrillin^{7, 8}. Independently of its composition, there is agreement that this surface amorphous layer helps to maintain a low friction coefficient during boundary lubrication⁶.

OA manifests by a depletion of proteoglycans, followed by break down of Type II collagen, mechanical failure and erosion of the articular cartilage². The concentration of calcium in healthy synovial fluids is ~ 2mM⁹, although values as high as 4mM have been reported¹⁰. There is some evidence for the prevalence of elevated calcium and phosphate contents in cartilage with progression of OA¹¹. Specifically, with progress from grade 1 to 3, the calcium content has been seen to increase by a factor of ~5. Recent works have also shown that the increased concentration in calcium-phosphate complexes in articular cartilage of early-stage OA¹² is responsible for cellular dysfunction.^{12, 13} A recent review reports that deposition of calcium pyrophosphate and basic calcium phosphate crystals is found in 100% of cartilage samples from patients with OA undergoing joint replacement surgery¹⁴. For crystallization to happen, the interstitial fluid must be supersaturated, thereby also supporting the exposure to elevated calcium and phosphate concentrations. A common symptom in OA is the

^a Materials Science and Engineering, University of Illinois at Urbana-Champaign, 1304 W Green St, Urbana, Illinois 61801, United States.

^b Department of Orthopedics, Rush University Medical Center, Chicago, IL.

^c Civil and Environmental Engineering Department, University of Illinois at Urbana-Champaign, Urbana, IL.

† Contributed equally

* Corresponding authors

Electronic Supplementary Information (ESI) available: [details of any supplementary information available should be included here]. See DOI: 10.1039/x0xx00000x

remodelling of the subchondral bone¹⁵, which can be accompanied by an increase of calcium and phosphate level in the subchondral milieu. Because articular cartilage gets most of nutrition from subchondral bone by diffusion, these changes in subchondral bone can affect the articular cartilage. It is also conceivable that because proteoglycans are lost during OA, less calcium can be stored in the tissue and more becomes available at the interface.

It is known that calcium can bind to negatively charged carboxylic groups of amino acids in collagen¹⁶ and to the glycosaminoglycans, *e.g.* of aggrecan¹⁷. Furthermore, due to its bivalency, calcium ions can crosslink molecules like collagen¹¹, aggrecan¹⁷, hyaluronan¹⁸ and cartilage oligomeric matrix protein¹⁹; a phenomenon commonly known as “ionic bridging”. While fluctuations of calcium concentrations have been associated with structural and mechanical changes of (dehydrated) cartilage^{20, 21}, the implications of calcium concentration to the hydrated cartilage surface has not been examined yet.

The objective of this study is to investigate the change of structural, mechanical and frictional characteristics of the articulating surface of healthy bovine cartilage induced by elevated calcium concentrations. Because macromolecular conformation is likely to change with the hydration state²², this work only considers hydrated cartilage. The combination of AFM imaging, eSFA and nanoindentation demonstrates the sensitivity of the cartilage’s surface to calcium beyond osmotic pressure effects. It is shown that the affinity of calcium to the surface amorphous layer results in an irreversible softening and swelling of the surface layer of $\sim 5 \mu\text{m}$ in thickness. This softening is accompanied by an increase in static friction and stick-slip upon increased calcium concentration and prolonged static loading, which should promote wear of the cartilage’s surface.

Results

Using a 3-mm biopsy punch, cylindrical cartilage plugs were removed from 6–8 months bovine stifle joints (see detailed Materials and Methods section). After freezing them at -20°C overnight, 8–12 μm sections from the *cartilage surface* of each plug were sliced with a cryostat (see cartoon in Fig. 1a). These sections were then kept in phosphate-buffered saline (1 \times PBS) at 4°C until the day of testing, but not more than 4 days. Attenuated total reflectance infrared (IR) spectroscopy was applied to evaluate the composition of cartilage’s articulating surface. Solutions of 0, 1.8 mM CaCl_2 and 10 mM CaCl_2 in 1 \times PBS were prepared and filtered to achieve different calcium contents in the cartilage sections after equilibration²⁰. Exposing cartilage to higher calcium concentration in the surrounding solution leads to increased calcium contents. For example, an increase in the cartilage calcium content by a factor of ~ 5 was achieved through the increase in calcium concentration from 2 to 10 mM²⁰. Here, the concentrations of 1.8 and 10 mM represent the calcium concentration in healthy synovial fluid and that found in cartilage tissue (unpublished observation by T.S.), consistent with the reported range 7–20 mM in the

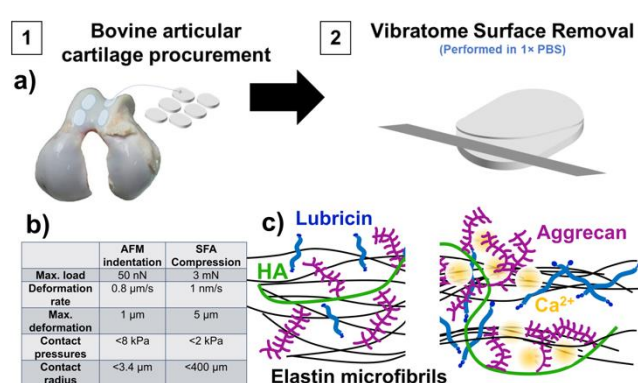


Figure 1. Sample preparation and experimental conditions for studies of the cartilage’s surface mediated by calcium. a) Preparation of cartilage sections. b) Conditions in indentation and compression experiments: maximum applied load, rate of deformation, maximum deformation, maximum contact pressure (P_{max}) and contact radius (a), a and P_{max} in AFM experiments were calculated based on Hertz model¹. The contact radius in eSFA was calculated with the deformation of the cartilage, considering that the geometry of two crossed-cylinders of radius R (2 cm) is equivalent to a sphere-plane for $R \gg D$, like here. For example, a compression of 4 μm in the normal direction implies a contact radius of $\sim 400 \mu\text{m}$. c) Cartoon showing the aggregation of the surface layer upon addition of calcium.

tissue^{23–25}. Tables S1 and S2 show the saturation index with respect to the calcium phosphate minerals that can precipitate under the selected conditions.

Structural and mechanical properties

Room temperature compression and decompression isotherms of the cartilage sections were measured at a rate of 1 nm/s using an extended Surface Forces Apparatus (eSFA). In eSFA experiments, the cartilage section is slowly compressed to exclude dynamic effects, while the resistive force to compression, the deformation of the cartilage section and its refractive index are measured with time. Before the measurements, the cartilage was equilibrated for ~ 12 hr in each solution. Two compression isotherms of the articular cartilage’s surface with an initial thickness of $H_0 \sim 12.4 \mu\text{m}$ in 1 \times PBS are shown in Fig. 2a (red represents approach and green is used for separation); the cartilage remained unstressed for 7 hr before the next compression started. Both the hysteresis between approach and separation and the decrease of the onset of repulsion during subsequent compressions reveal a change of the cartilage’s surface structure upon compression. It cannot be ruled out that longer equilibration times under unstressed conditions could yield a full recovery of the microstructure²⁶. However, the observation time in other mechanical tests is typically much smaller. The reduction in the onset of the repulsion of $\sim 1 \mu\text{m}$ implies the decrease in cartilage thickness to $H \sim 11 \mu\text{m}$. Upon consecutive compressions in 1.8 mM CaCl_2 , the change in the cartilage’s thickness (Fig. 2b, $H \sim 11.3 \mu\text{m}$) and the hysteresis is less prominent, *i.e.* the behavior becomes more elastic. Reference measurements in DI water confirmed the irreversibility of the initial compression, while the variation between compression isotherms in subsequent measurements (in water in Fig. S1 or in 1 \times PBS in Fig. 2a) is mitigated, indicating a more stable microstructure. Despite this, when the cartilage is equilibrated in 1 \times PBS with 10 mM CaCl_2 , the onset of the repulsion remarkably increases in consecutive compression

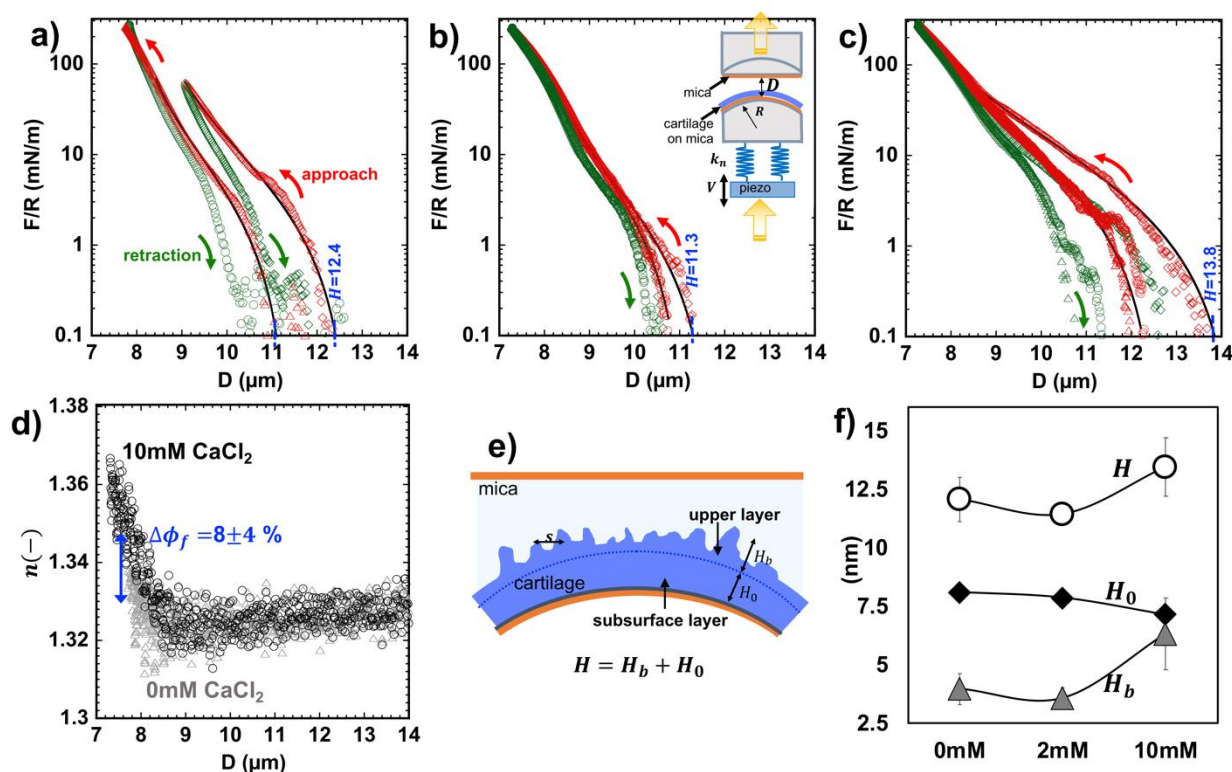


Figure 2. Compression isotherms as a function of varying ionic strength. Compression isotherms as a function of the separation between mica surfaces (D) (approach in red and retraction in green) in $1\times$ PBS with a) 0mM, b) 1.8 mM and c) 10 mM CaCl_2 . The inset in b) shows the schematics of the eSFA for the cartilage experiments (cartilage in blue, mica with silver mirror on the back side in brown). The lines show the fits of Eq. (3) to the experimental results. d) Representative measurements of the refractive index of the confined film between mica surfaces upon compression of the cartilage in $1\times$ PBS with 0 (grey triangles), and 10 mM CaCl_2 (black circles). An increase in refractive index reflects the decrease in water content upon compression. e) Cartoon of the articulating surface investigated by eSFA, showing the soft surface layer of thickness H_b and a less compressible layer underneath of thickness H_0 . The fitting parameters of Eq. (3) are shown in f). The error bars are sometimes smaller than the markers size, and therefore, not always visible.

isotherms and the hysteresis becomes more prominent (Fig. 2c, $H\sim 13.8$ μm). This points towards a remarkable structural change of the cartilage's surface.

The compressive modulus (B) can be roughly estimated from the compression isotherms assuming an elastic behavior²⁷, according to:

$$\frac{F}{R} = \frac{\pi B(D-H)^2}{H} \quad \text{Eq. (1)}$$

The fit of Eq. (1) to the experimental results is possible for the initial compression of ~ 1 μm (see Fig. S2 in the SI) and it provides the value of B , which decreases from 7.1 ± 0.6 kPa to 6.2 ± 1.5 kPa upon addition of 1.8 mM CaCl_2 to $1\times$ PBS, and to 5.9 ± 0.8 kPa with 10 mM CaCl_2 . Note that these values are of the same order of magnitude compared to reported elastic moduli of the hydrated cartilage's articulating surface⁵.

The cartilage surface was imaged by Atomic Force Microscopy (AFM) in Quantitative Imaging (QI) mode after equilibration in the prepared solutions. Fig. 3a-h shows representative images of the cartilage's surface immersed in $1\times$ PBS with different concentrations of CaCl_2 at two different magnifications. The surface microstructure is distinct from the subsurface (*cf.* Fig. 3l). The images reveal a coarse and branched network in $1\times$ PBS (Fig. 3a) with a diameter of $d\sim 317\pm 84$ nm ($n=30$), *i.e.* much larger than that of the collagen fibers in the subsurface ($d\sim 23.8\pm 7$ nm, $n=94$, Fig. 3l). Higher magnification images reveal a granular microstructure in $1\times$ PBS (Fig. 3e),

which agrees qualitatively with reported AFM images of the cartilage's surface^{5, 7, 28}. IR spectroscopy reproducibly confirms the presence of proteoglycans in the cartilage's sections and their smaller concentration toward the surface; see a detailed explanation of the results in the SI (Fig. S3). Furthermore, although the infrared absorption spectra of collagen and elastin are quite similar, IR measurements support the presence of elastin, and hence, the coarser network could be also composed of elastin fibers, which have been reported to have diameters of up to ~ 1 μm ²⁹.

Upon equilibration in 1.8 mM CaCl_2 , the diameter of the network appears thicker (roughly $d\sim 415\pm 95$ nm, $n=21$). This is much more prominent in 10 mM CaCl_2 ($d\sim 1624\pm 846$, $n=18$) and it demonstrates the significant aggregation of the macromolecular network with a simultaneous increase in RMS roughness and in void size ξ (see caption in Fig. 3). This is concurrent with the swelling and softening inferred from SFA experiments at this concentration. Overnight re-equilibration in $1\times$ PBS (0 mM CaCl_2) does not induce a complete recovery of the surface structure (Fig. 3d;h), which indicates that the influence of CaCl_2 on the properties of the cartilage's surface is irreversible within the duration of these experiments. The trends are reproducible on different regions of the articular cartilage's surface. Although mineral precipitation is possible (Table S1-S2), AFM imaging showed that the cartilage's surface remained free of crystals. Macromolecules can affect

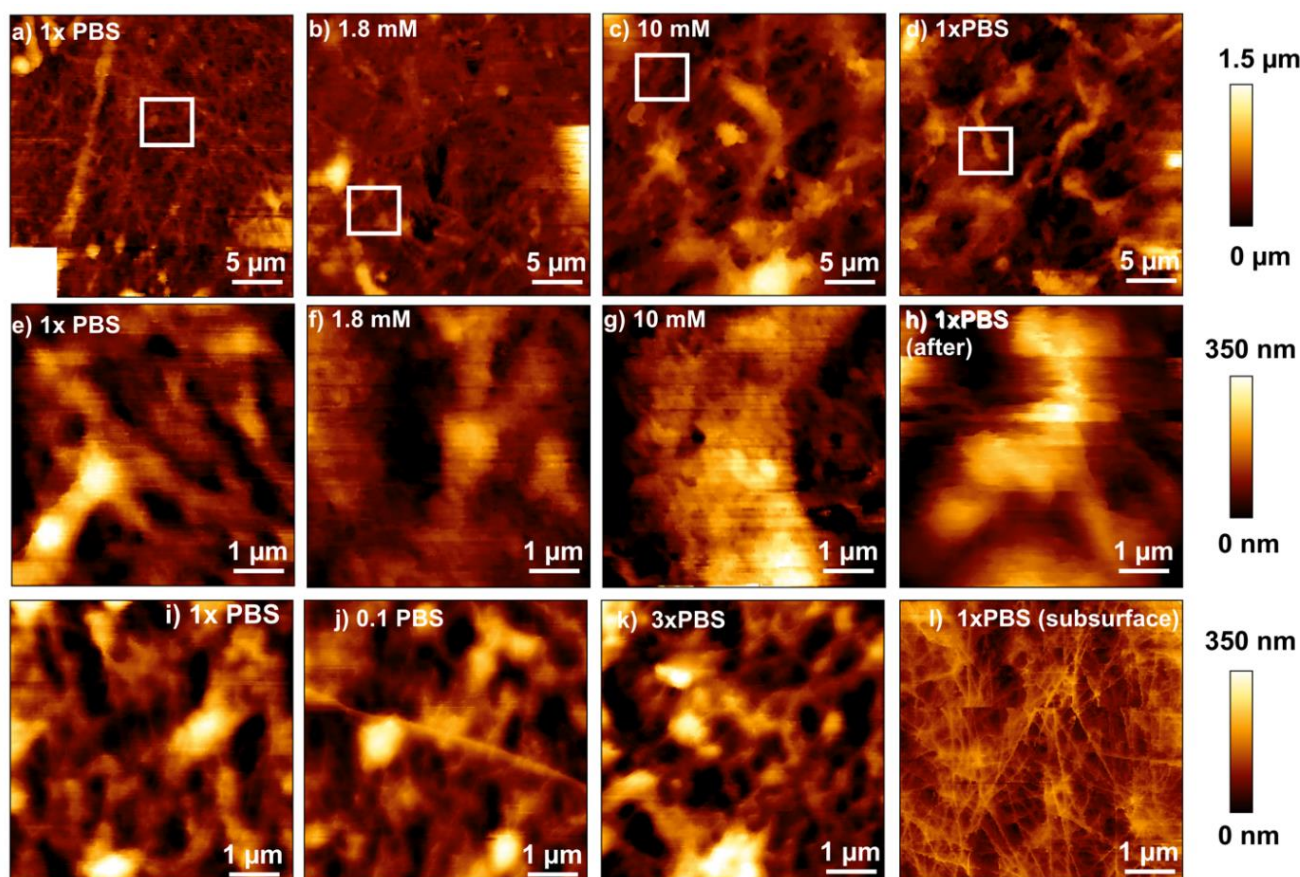


Figure 3. Images of cartilage's articulating surface as a function of calcium concentration. QI images of the cartilage surface equilibrated for 5 hr in a;e) 1× PBS and 1.8mM CaCl₂, b;f) 1× PBS and 1.8mM CaCl₂, c;g) 1× PBS and 10mM CaCl₂ and d;h) re-equilibration in 1× PBS (denoted "after"), respectively. First row at low magnification (30 μm × 30 μm) and second row at higher magnification (5 μm × 5 μm). RMS roughness: (a) 278±34 nm, (b) 182±38 nm, (c) 243±50 nm, (d) 267±35 nm while (e) 97±39 nm, (f) 49±10 nm, (g) 133±28 nm and (h) 137±22 nm. Aggregate thicknesses: (a;e) 298±68.3 nm, (b;f) 415±95.16, (c;g) 1624±846 and (d;h) 1865±533 nm. Void size (ξ): (a;e) 819±175 nm, (b;f) 1388±371, (c;g) 1485±410, (d;h) 1611±321 nm. QI images of the cartilage surface equilibrated for 5 hr in i) 1× PBS, j) 0.1× PBS and k) 3× PBS, as reference. l) Image of the cartilage subsurface; the average collagen diameter is 26±6 nm obtained from n=25 fibers per image in 4 images. The scale bars are shown in each diagram. Cantilever stiffness=0.3 N/m. Nominal tip radius= 30 nm.

nucleation; they can both inhibit and promote it. For instance, calcium binding to aggrecan has been reported to prevent mineralization in cartilage³⁰. Nevertheless, the nanosized precipitate could be difficult to image within the complex matrix structure, or it could precipitate underneath the surface, and hence, we do not have evidence to fully support or rule out precipitation at this point.

Reference images were also taken at different dilutions of PBS, *i.e.* 0.1× PBS, 1× PBS and 3× PBS, in the absence of calcium (Fig. 3i-k). Increasing the ionic strength to 3× PBS does not lead to aggregation of the solid matrix. Instead, the surface roughness increases from 149±10.0 nm to 194.9±56.7 nm with the decrease in dilution from 0.1×PBS to 3×PBS, which suggests that a partial dehydration of the cartilage might have taken place. In fact, an increase of the ionic strength in the cartilage's external environment (*i.e.* from 0.1× to 3× PBS) is expected to cause a loss of extrafibrillar water in the cartilage to balance the osmotic pressure gradient³¹. This dehydration can also happen in the cartilage's surface layer, as glycoproteins (*e.g.* lubricin) and proteoglycans (hyaluronan) are highly negatively charged. In contrast, the changes illustrated in Figs. 2 and 3 when calcium is added cannot be attributed to osmotic pressure effects.

Representative SFA measurements of the refractive index (n) are shown in Fig. 2d. The refractive index is a measure of the density of the film³² and it can be roughly modeled according to:

$$n(D) = n_c - \phi_f(n_c - n_f) \text{ Eq. (2)}$$

where $n(D)$ is the refractive index as a function of surface separation, n_c is the refractive index of the solid matrix ($n_c=1.53$, for collagen), $n_f=1.337$ is the refractive index of water, and ϕ_f is its volume fraction. When the cartilage is compressed to less than $\sim 9 \mu\text{m}$, the refractive index notably increases at all solution conditions. Hence, the increase in refractive index is due to the remarkable loss of water in the cartilage upon compression. The fit of Eq. (2) to the measured refractive index gives a reduction of the water content in cartilage of $\sim 8 \pm 4 \text{ vol}\%$ with an increase in CaCl₂ concentration from 0 to 10 mM. A loss of water with increase in ionic strength is expected to balance the osmotic pressure between the extrafibrillar water and the external environment of the cartilage, and hence, these results are reasonable. However, the compression from 14 to 9 μm does not cause any variation of the refractive index, which remains very close to that of water under the investigated conditions. This implies that the *top*

surface layer has a very high water content (>95%), like a gel or a brush. Note that the refractive index of the cartilage's superficial zone has been reported to be 1.361 ± 0.032 ³³, and hence, in reasonable agreement with our results considering the precision of the refractive index measurements.

Although the Alexander-de Gennes model³⁴ is only strictly valid to describe the compression of long neutral polymer brushes, it has been shown to describe well the behavior of charged macromolecules like lubricin and hyaluronan grafted via fibronectin to a substrate in aqueous environment³⁵. In our case, satisfactory fits to the compression of the cartilage's articulating surface are only achieved *via* a modified model that assumes the presence of a compressible, thermally mobile, well-hydrated surface layer and a much less deformable region underneath (see schematics in Fig. 2e). This model gives the resistive force to compression (F) normalized by the radius (R):

$$\frac{F}{R} = \frac{8\pi k_B T \cdot H_g}{35\Gamma^{3/2}} \left(7 \left(\frac{H_g}{D-H_0} \right)^{5/4} + 5 \left(\frac{D-H_0}{H_g} \right)^{7/4} - 12 \right) \text{ Eq. (3)}$$

H_g being the thickness of the soft surface layer with a solid surface density Γ , H_0 the thickness of the less compressible layer underneath (subsurface), and hence, $H = H_g + H_0$ is the cartilage's section thickness, *i.e.* the onset of the repulsion. The black lines in Figs. 2a-c demonstrate the good agreement between the experimental results and the model.

The fits to the experimental results provide H_0 and H_g . The soft surface layer slightly collapses from $H_g = 4.0 \pm 0.5 \mu\text{m}$ to $3.5 \pm 0.5 \mu\text{m}$ upon addition of 1.8 mM CaCl_2 , but it notably expands in 10 mM CaCl_2 to $H_g = 6.2 \pm 1 \mu\text{m}$. In contrast, with increase in calcium concentration, the subsurface layer gradually collapses from $H_0 \sim 8$ to $\sim 7 \mu\text{m}$, which is consistent with the increase in osmotic pressure with higher concentration. Fig. 2f suggests that the observed increase in refractive index with CaCl_2 concentration may be associated with the contraction of the subsurface layer, since the surface layer swells, and hence, it becomes more hydrated in 10 mM CaCl_2 . The eSFA experiments thus reveal the graded response of the cartilage's surface, *i.e.* of the surface ($\sim 5 \mu\text{m}$ in thickness) and subsurface layers and their different responses to calcium concentration. The graded structure of the cartilage's surface amorphous layer – composed of a gel-like layer on top of a granular stiffer layer – was first proposed by Crockett et al. based on AFM images⁵.

To determine the influence of calcium concentration on the Young's modulus of the cartilage's articulating surface, nanoindentation measurements were carried out by AFM with silica colloids (diameter = 20 μm) at 0.8 $\mu\text{m/s}$ and indentation depths smaller than 1 μm (see Fig. S4). Experimental conditions in eSFA and nanoindentation are compared in Fig. 1b. In contrast to SFA, indentation maps were measured on the pristine cartilage surface, and hence, the influence of multiple compressions was not investigated by AFM. The indentation depth (d) is smaller than 1 μm , and therefore, only the topmost surface layer is probed here. A deviation of the experimental data from the Hertz model was systematically observed close to the surface (Fig. S5). Inspired by recent work on hydrogels³⁶, the Hertz model was then fit to the experimental results

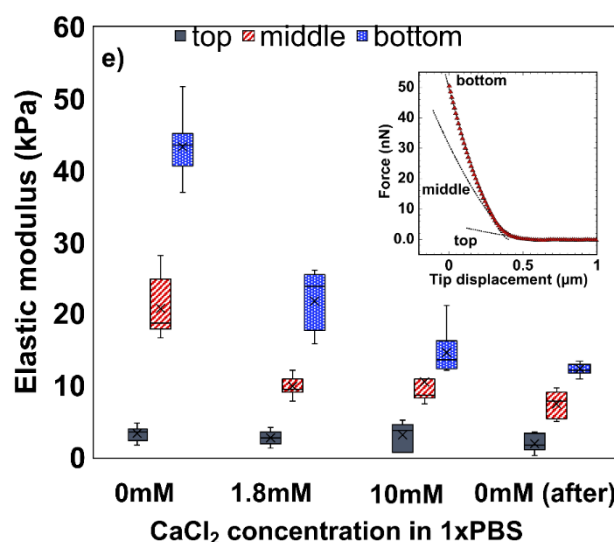


Figure 4. Elastic modulus of the cartilage's surface and subsurface as a function of calcium concentration. Elastic modulus according to the Hertz model as a function of CaCl_2 in 1x PBS. The Hertz model was applied "piecewise" to determine top, middle and bottom moduli. The inset shows the definition of the elastic modulus as a function of depth. The decrease of the elastic modulus with calcium concentration is more prominent in middle and bottom regions; this is not seen when comparing 1x PBS and 3x PBS in reference measurements (Fig. S6). Cantilever stiffness = 0.4 N/m. Radius of colloid = 10 μm .

"piecewise" (see lines in inset of Fig. 4). This practice led typically to three elastic moduli on each indentation curve, which is indicative of the nonlinear elastic behavior of the cartilage's surface (Fig. 4). For example, the elastic moduli are 3.3 ± 1 kPa, 20.7 ± 3.9 kPa and 43.5 ± 4.6 kPa in 1x PBS with an increase in indentation depth. Addition of calcium leads to a gradual decrease in the elastic moduli and there is no recovery upon re-equilibration in 1x PBS, which let us denote this weakening as "irreversible". This is in contrast to reference measurements in 3x PBS (Fig. S6).

In the presence of calcium, jumps happen upon indentation, making it difficult to fit the model to the experimental results (see arrows in Fig. S4). These jumps reflect sudden ionic bridging between the colloid and the negatively charged macromolecules. Importantly, after re-equilibration in 1x PBS, the small jumps in the indentation curves remain, which demonstrates that the calcium is still present in the cartilage. Note that a quantitative comparison between the moduli obtained by eSFA and nanoindentation is not possible due to various reasons. First, eSFA experiments are carried out in *quasi* equilibrium, which mitigates poroelastic effects³⁷ on the resistance to compression, in contrast to AFM indentation. Second, the contact radius is as large as 400 μm in eSFA while it is less than 3.4 μm in AFM, and hence, the length scales are also very different; the indentation depth in AFM is less than 1 μm compared to more than 4 μm in SFA experiments. Third, calcium does not bind to mica at such low concentrations³⁸, which explains the absence of jumps in the SFA force curves upon retraction. Despite these differences, a weakening of the cartilage's surface with an increase in calcium concentration is inferred from both AFM and SFA.

Tribological behavior of the articulating surface

To evaluate the tribological implications of these results, friction-force measurements were carried out in 1× PBS with 0 and 10 mM CaCl₂ with a silica colloid as the countersurface. The static loading time before the silica colloid was laterally pulled at 1 μm/s was varied between 5 s and 50 s. Fig. 5a shows the lateral force as a function of the position of the cantilever at various loading times in 1× PBS under a normal load of 50 nN. The prominent peak corresponds to the static friction or stiction, *i.e.* the friction force at the commencement of sliding, after which friction decreases to the dynamic value. The inset in Fig. 5a reveals that the static friction increases with the increase in the hold time in 1× PBS. In contrast, short loading times (≤5 s) lead to negligible stiction to the silica surface. The static friction coefficient (μ_s) is almost one order of magnitude larger than the dynamic coefficient of friction, μ_d (μ_s goes up to 0.016 vs. $\mu_d \sim 0.003$). The relative constant dynamic friction coefficient over the sliding distance reflects the smooth motion of the colloid, while its small variation is likely due to the heterogeneity of the cartilage's surface. Importantly, the dynamic friction coefficient of the cartilage's subsurface (Fig. 21) is $\mu_d \sim 0.02$, *i.e.* one order of magnitude larger, which reflects the lubricious properties of the articulating surface.

Fig. 5b shows the measured lateral force while the colloid slides along the cartilage's surface in 1× PBS with 10 mM CaCl₂. The sudden jumps of the lateral force indicate that the colloid does not slide smoothly, but instead, it moves intermittently; this is also called stick-slip motion³⁹. Here, the colloid sticks to the cartilage due to the high adhesion, and when the lateral force is large enough, the colloid detaches from the cartilage, then it slides until it sticks again. The initial stiction peaks are of greater magnitude in the presence of calcium; μ_s is about three times larger than in Fig. 5a. Furthermore, the stick-slip becomes notorious at all investigated loading times. Such stick-slip may be directly related to the ionic bridging between the silanol groups and the molecules in the cartilage's articulating surface mediated by calcium, as silica is negatively charged at neutral

pH⁴⁰ and binds to calcium⁴¹. In addition to this, the effect of the loading time is less clear than in 0mM CaCl₂, suggesting that calcium bridging between cartilage and silica mitigates the influence of the static loading time.

Discussion

This experimental study supports the presence of a surface layer in the articulating surface of bovine cartilage with a thickness of ~ 5 μm, a very high water content and higher compressibility than the layer underneath. According to nanoindentation, the elastic modulus of the cartilage's articulating surface increases with depth by roughly one order of magnitude from 3.3 to 43 kPa. AFM images of the cartilage's surface in 1× PBS reveal a granular microstructure within a coarse fibrous network, with fiber diameters much larger than that of the collagen fibers in the subsurface region. This may be due to the deposition of proteoglycans onto collagen fibrils, as reported for mice articular cartilage²⁸; and/or to the presence of a network of coarse elastin-rich fibers⁷. Although the presence of collagen is not obvious in these images, it cannot be excluded that both elastin and collagen fibers are part of the hydrated and swollen matrix, together with proteoglycans and glycoproteins, based on IR spectroscopy.

The origin for the hysteresis and lack of recovery upon slow and unconfined *initial* compression in eSFA experiments is intriguing. One possible explanation is that the content of proteoglycans is low, as they are mainly responsible for the re-swelling of cartilage³¹; this is supported by the graded composition revealed by IR spectroscopy. In addition to this, the prominent squeeze-out of fluid could promote intermolecular interactions. This is reminiscent of the self-adhesion between aggrecan molecules when subjected to static compression for sufficient long periods of time⁴². Note that this happens despite the strong electrostatic repulsion between the highly negatively charged glycosaminoglycan. Hydrogen bonding, hydrophobic interactions between the methyl groups and carbon rings as

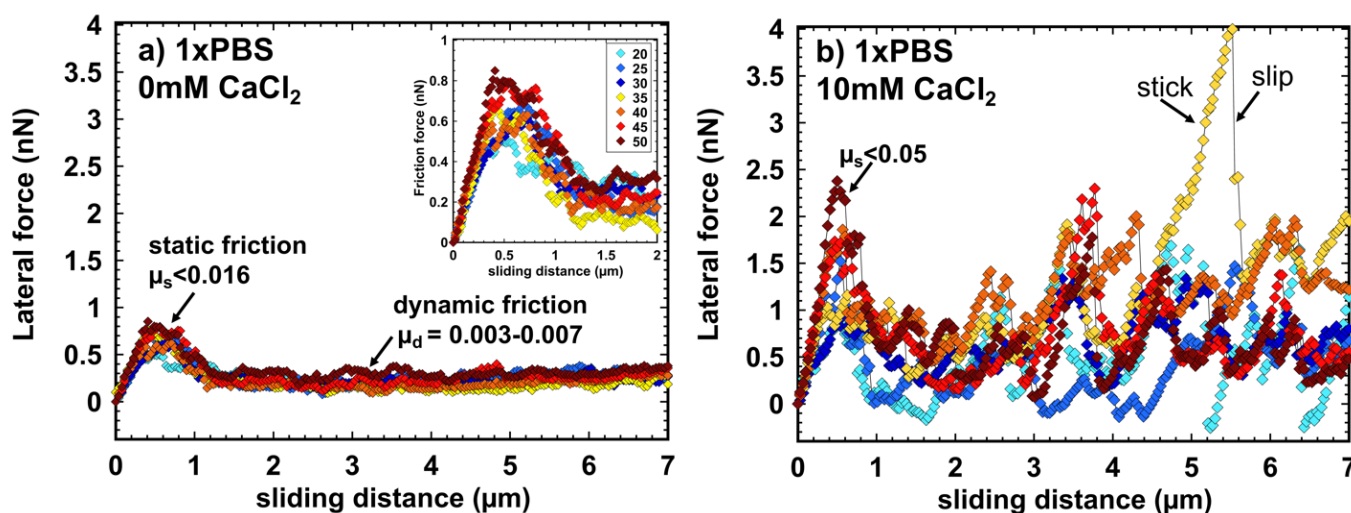


Figure 5. Lateral force vs. sliding distance between a silica colloid and articulating surface of cartilage. The lateral force was measured upon a constant load of 50 nN at selected hold times between 20 and 50 s, in a) 1× PBS and b) 1× PBS with 10 mM CaCl₂. The arrows in b) help visualize a stick and slip event. The colour legend in both diagrams is shown in the inset of a). Sliding velocity= 1 μm/s. Cantilever stiffness=0.45 N/m. Radius of colloid= 10 μm. The coefficients of friction were determined at loads between 20 and 50 nN.

well as physical entanglements between the glycosaminoglycan side chains are proposed as relevant factors contributing to aggrecan self-adhesion. Similar intermolecular bonding upon removal of water has been proposed for other carbohydrate-rich macromolecules and proteins⁴³ and between hyaluronan and lipids^{44,45}.

The increase in static friction with static loading time supports that time-dependent interactions (here, between cartilage's surface and silica) are relevant. A recent study of hydrogel's static friction has revealed that two main phenomena explain the increase of static friction³⁶. First, the contact area increases with time due to the gradual drainage of the imbibed fluid. Second, the interfacial shear strength increases with loading time owing to the gradual adsorption of the polymer network to the silica colloid (e.g. via hydrogen bonding), which is promoted by water exudation. Since cartilage is a biphasic material composed of an interstitial fluid and bio-macromolecules, the same mechanisms are expected to be relevant. In fact, various studies have showed that prolonged static (non-sliding) loading leads to the squeeze-out of the fluid from cartilage's superficial zone^{46,47}, and thereby to an increase in adhesion and friction⁴⁷.

Given the significant aggregation of the solid matrix shown in the AFM images, it is possible that calcium mediates crosslinks between negatively charged molecules present in the surface amorphous layer. Interestingly, the self-adhesion between aggrecan molecules was also found to significantly increase with calcium concentration due to ion bridging of the glycosaminoglycans under static loading⁴². A similar behavior could be also expected for small proteoglycans, like decorin, which could bridge between collagen fibrils under static loading. Such enhanced interactions between macromolecules under compression can thus qualitatively explain the hysteresis between compression and decompression and that hysteresis becomes less prominent in subsequent compressions.

Collagen contains positively, negatively charged and polar but uncharged amino acids. The positive charge carried by arginine and lysine is believed to play an important role in the electrostatic interactions between collagen molecules, and thereby, in the self-assembly and stability of the collagen fibrils⁴⁸. Calcium ions can bind to the carboxylic groups, and thereby, bridge adjacent collagen molecules and alter collagen self-assembly¹⁶. This is consistent with the reported thickening of collagen fibrils in the presence of calcium¹¹, although the reported diameter is much smaller than in our AFM images. On the other hand, elastic fibers consist mainly of an elastin core and fibrillar glycoproteins, like fibrillin. While it is not clear yet how calcium binds to elastin and how it affects its properties, fibrillin has multiple calcium binding domains, and its structure and mechanical properties depend strongly on calcium concentration⁴⁹. The lateral packing of fibrillin monomers is reported to be calcium dependent; fibrillin adopts a more curved conformation and its stiffness increases with calcium concentration⁵⁰. Although the incubation with EDTA results in significant disruption of microfibril morphology, the change is shown to be reversible on providing calcium at even much higher concentrations than in the present study, indicating that

changes of calcium do not compromise microfibrillar integrity⁵⁰. While this behavior alone cannot explain our results, it demonstrates the binding capability of calcium to elastic fibers and the possibility to crosslink adjacent proteoglycans like decorin.

Lubricin, a mucin-like glycoprotein with lubricating properties, is also present on the *lamina splendens* of articular cartilage and in synovial fluid^{51,52}. The end-protein domains of lubricin stick to many molecules, including hyaluronan and collagen, while the highly glycosylated mucin domains remain strongly hydrated. A recent study has shown that a calcium concentration above 5 mM causes structural and mechanical changes of lubricin brush layers adsorbed on silicon oxide substrates¹⁰. Calcium thus binds to carboxylate, which leads to a partial brush dehydration and densification, as well as to a partial collapse of the glycans, while both protein-end domains remain firmly stuck to the substrate. This results in certain aggregation and in an increase in brush roughness. Furthermore, while the elastic modulus of the mucin domains increases with calcium concentration (from 0.2 to 0.8 kPa), the end-domains become softer (from 22–34 kPa to 20–26 kPa). This has been associated with the denaturation and unfolding of the end-protein groups. Interestingly, this behavior agrees qualitatively with the observed softening of the cartilage's surface observed in our experiments. In contrast, hyaluronan remains strongly hydrated and without appreciable conformational changes even at calcium concentrations 20-fold larger than in our study⁵³. It appears that the hyaluronan molecules preserve extended linear regions, implying that coiling and entanglement are hindered, and thereby, relaxation and compressibility behavior stay unchanged. The response of hyaluronan to calcium is essentially of osmotic origin due to electrostatic screening, and hence, this alone cannot explain the observed behavior of the cartilage's surface.

It is, however, challenging to extrapolate the calcium-induced response of single molecules to tissue micromechanics. From a microstructure perspective, the aggregation of the solid matrix upon addition of calcium reveals an increase in the void size ξ , which is concurrent with the increase of the compressibility of the top surface layer and its swelling. Hydrogels are biphasic materials composed of a macromolecular network and large amounts of water, and hence, their structure has some similarity to that of cartilage. In the context of hydrogels' scaling theory⁵⁴, the elastic modulus scales as ξ^{-3} , ξ being the mesh size, and its swelling ratio, $Q \sim \xi^3$. Thus, an increase in mesh size yields both softening and swelling of hydrogels. Accordingly, the observed rearrangement of the solid matrix upon addition of calcium could also physically explain the observed softening and swelling of the surface layer.

The tribological implications are also worth discussing. The stick-slip motion in the presence of calcium suggests that the macromolecules in the surface layer stick to silica and are stretched and pulled, as the colloid slides. This should equally happen on cartilage-cartilage tribopairs, although the strength of the adhesive forces will be obviously different. Note that this happens at contact times ($t_V = a/2V \sim 1$ s) that are smaller than the static loading times that yield stiction in the absence of

calcium ($t_s > 5$ s). As discussed above, high calcium concentrations also lead to the softening of the surface layer. This suggests that the synergy between the weakened cartilage's surface and the adhesion to negatively charged counterfaces, both promoted by calcium, might be a mechanism that promotes wear and damage of the cartilage surface as a result of elevated calcium content in the cartilage surface. In fact, several studies have loosely related high adhesion and friction of articular cartilage to joint fatigue and wear of the cartilage's surface^{47, 55, 56}.

Conclusions

A symptom common to many joint diseases like OA includes the precipitation of calcium phosphate crystals. During the course of osteoarthritis, calcium homeostasis may thus be disturbed and there are many factors that can affect the generation of calcium crystals including the concentration of anions like urate, pyrophosphate and phosphate, temperature, pH and as well as macromolecules that inhibit or enhance mineral nucleation and growth. Here, we used a simple system with calcium and phosphate buffers and the devitalized healthy cartilage surface to exclude the complication of chondrocyte metabolism and structural damage due to OA. Previous to the loss of the structural integrity of the cartilage at the onset of OA, a softening of the cartilage surface (in equilibrium with PBS) has been observed at the nanoscale. This work shows that an elevated calcium concentration in the cartilage's surface could justify a softening of the surface amorphous layer and increased stiction. It is also worth noting, that our work does not support the previously proposed relation between elevated calcium concentration in human AC with nanoscale stiffening that was observed at the onset of OA⁵⁷. We believe that the reason for this discrepancy as well as the much higher moduli in that work (~1 GPa) rely in the different hydration state of the cartilage, since that previous work carried out nanoindentation on dehydrated cartilage. In the future, it will be important to assess cartilage calcium levels in human subjects and test the hypothesis that a disturbed calcium homeostasis is responsible for OA initiation.

Materials and Methods

Cartilage sample preparation

Bovine stifle joints (age 6-8 months) were obtained from a local abattoir and opened to reveal the trochlear groove. Cartilage integrity was assessed, and joints that had cartilage that exhibited exposure to blood and/or bruising were excluded. Using a 3-mm biopsy punch, cylindrical cartilage plugs were removed from the joint. The plugs were then placed into optimal cutting temperature (OCT) compound, with the surface-side of the cartilage plug as the sectioning plane, and frozen at -20°C overnight. The following day, 8-12 µm sections from the cartilage surface of each plug were obtained with a cryostat. Phosphate-buffered saline solution (1× PBS) was prepared by diluting 10× PBS (no calcium, no magnesium,

14200075, ThermoFisher). After each section was cut, it was placed in 2 mL of 1× PBS. The surface was deemed captured when a cartilage section became apparent after gentle rinsing in the saline solution. These samples were then kept in 1× PBS solution at 4°C until the day of testing. Although the sections underwent 1 freeze-thaw cycle, several studies have found that cartilage mechanical properties do not change after a single freeze-thaw cycle^{58, 59}.

Medium

Solutions of 1× PBS with 0 mM, 1.8 mM CaCl₂ and 10 mM calcium chloride (CaCl₂) were prepared with CaCl₂ from Sigma Aldrich. Before use, all solutions were filtered using a 0.22 µm polyamide filter. At the selected concentrations, the solution was supersaturated with respect to various calcium phosphate minerals as shown by their saturation index calculated with the software Visual MINTEQ v. 3.1. AFM imaging showed that the cartilage's surface remained free of crystals during the duration of the experiments. Note that calcium binding to aggrecan has been reported to prevent mineralization in cartilage⁶⁰.

Attenuated Total Reflectance Infrared Spectroscopy

Attenuated Total Reflectance Infrared Spectroscopy (ATR-IR) (PerkinElmer, Frontier, and Pike Technologies, GladiATR with a diamond crystal) was used to determine the chemical footprint of the cartilage samples. Cartilage samples equilibrated in 1× PBS were placed on the ATR crystal and a light pressure was applied with the help of the sample press knob to enhance the signal. The sample absorbance was collected in the range 400-4000 cm⁻¹ and the Spectrum software was used to correct the measurements with the baseline of 1× PBS to determine the signal of the solid matrix. The penetration depth of the IR beam into the sample can be estimated according to:

$$d_p = \frac{\lambda}{2\pi(n_1^2 \sin^2 \theta - n_2^2)^{1/2}}$$

where θ is the angle of incidence (45°), n_1 the refractive index of the ATR crystal ($n_1 = 2.4$ for diamond), n_2 the refractive index of the cartilage ($n_2 \sim 1.36$ for the superficial zone), and λ the wavelength of the IR beam. In the range of interest of wavenumbers (λ^{-1}) from 900 to 1800 cm⁻¹, the penetration depth ranges from 1.1 to 2.2 µm.

At least two IR spectra were taken for each sample orientation, *i.e.* with the surface of the cartilage section in contact with the ATR crystal (labelled as "top" interface), and with the bottom surface in contact with the ATR crystal (labelled as "bottom" interface).

AFM imaging

Cartilage surfaces were imaged by Atomic Force Microscopy (Nano Wizard, JPK Instruments, Germany) using quantitative imaging mode (QI) with a sharp tip (HQ:CSC37, No Al, 0.3-0.9 N/m, Nanoandmore, USA). In QI mode, cross-sections (30 x 30 µm and 5 x 5 µm) are divided into a grid of 256 x 256 pixels and force-distance curves are measured at each pixel at an approach speed of ~ 60 µm/s and a very small load of ~1 nN. The force curves are converted into a topographic image of the surface. Note that QI is not an indentation measurement but an imaging technique, where the tip applies a very small force on the surface for a very short period of time. This feature is

especially useful for imaging soft materials as it prevents application of lateral force, and hence, artifacts due to drag. The raw images were post-processed using JPK software by subtracting a polynomial fit from the surface and replacing empty pixels by interpolation.

Extended Surface Forces Apparatus (eSFA)

Compression and decompression isotherms were obtained using an eSFA, a modified version of the Mk III SFA (Surforce, Santa Barbara, CA),⁶¹ with attachments to improve the accuracy, resolution, mechanical drift, thermal stability, imaging, and essential automation of the instrument; these modifications are described in detail in the literature^{62, 63}. The transmitted interference spectrum consists of fringes of equal chromatic order that are analyzed by fast-spectral-correlation interferometry to evaluate the surface separation (D) and the refractive index (n) simultaneously. Uniformly thick mica sheets with a thickness between 2 and 5 μm were prepared by manually cleaving ruby mica of optical quality (grade 1; S&J Trading, New York, NY) in a class-100 laminar-flow cabinet. The mica sheets were cut to a size of 1 cm x 1 cm using surgical scissors to avoid possible contamination with nanoparticles. A silver film of 40 nm thickness was thermally evaporated onto mica sheets in vacuum (2.10^{-6} mbar). The silver-coated mica sheets were glued onto cylindrical lenses with a resin glue (EPON 1004F). The samples were then immediately inserted into the sealed eSFA, the fluid cell was purged with dry nitrogen, and the mica thickness was determined by means of thin-film interferometry in mica-mica contact. Immediately after this measurement, only one of the glass discs was disassembled to graft the cartilage section on mica, while the countersurface was kept as bare mica in the experiments.

Solutions of 10 wt% albumin in 1 \times PBS and 5 vol% glutaraldehyde in 1 \times PBS were mixed in a 1:1 ratio and the resulting solution was used to glue the cartilage section onto the mica. 500 μL of the glue solution was pipetted onto the mica surface and a tissue (Kimwipe, Kimberly-Clark Kimtech Science) was used to absorb excess solution so that only a thin layer of the glue solution remained on the surface. This mixture has been used extensively as a tissue adhesive⁶⁴. The thickness of this glue layer was determined to be less than 90 nm by multiple-beam interferometry⁶⁵. Immediately after this, the cartilage sections were transferred onto the mica surface with the help of blunted-tip tweezers. The glass disc with the cartilage was kept in a closed clean petri dish inside the laminar flow cabinet for a minimum of four hours to allow the binding of cartilage to the mica surface. After the initial 30 minutes, a droplet of 1 \times PBS was placed on the surface of the cartilage section to avoid dehydration. After four hours, the disc with the cartilage grafted on mica was placed back into the eSFA and the fluid cell was filled with 1 \times PBS for equilibration. Then, the point of closest approach (PCA) was readjusted with a precision of $\pm 1\mu\text{m}$ in the lateral direction. The accuracy of the measurement of surface separation (D) at the PCA is typically ± 30 pm, but it is ± 5 Å here due to the large thickness of the cartilage samples ($\sim 10\mu\text{m}$). The precision of the refractive index measurement was determined to be ~ 0.03 .

Slow compression and decompression of the cartilage sections at constant rate (V) of 1 nm/s were performed at least three times per solution at constant temperature (298 ± 0.1 K). First, 1 \times PBS solution was injected into the fluid cell until complete immersion of the two surfaces (mica vs. cartilage). The experiments with each cartilage section started with 1 \times PBS, and then, the concentration of CaCl_2 was increased stepwise from 0 to 1.8 mM, and then, to 10 mM; 10 mM was the mean calcium concentration measured in this tissue. Reference measurements were carried out in DI water. To ensure a thorough solution exchange, the two surfaces were first separated to $D > 50\mu\text{m}$ and then the liquid in the fluid cell was depleted and refilled 3 times with the new solution to ensure exchange. Drying of the cartilage did not happen during the exchange of the solution as a drop of solution was maintained between the two surfaces. The compression started after re-equilibration for at least 12 hours. The refractive index (n) and the separation between the two mica surfaces at the PCA (D) were measured in real-time with an acquisition rate of at least 1 Hz. The spring force can be obtained from $F = k_n(D - D_0 + Vt)$, where D_0 is the initial separation at which the net force is zero and t the point of time. Since the Debye length of the selected solutions is smaller than 1 nm⁶⁶, the electrical double layer force is of short range and can be ignored. Hence, the thickness of the cartilage was determined from the onset of the increase in repulsion (H) and the measured force is attributed to the resistance to the compression of the cartilage. A spring constant of 2340 ± 60 N/m was used in this work.

Colloidal probe AFM for nanoindentation and friction force measurements

An AFM (Nano Wizard, JPK Instruments, Germany) was used for colloidal probe indentation and friction-force measurements. All measurements were conducted with silica colloids of nominal radius equal to 10 μm (Duke Scientific, Thermo Scientific, USA). The colloids were attached to the end of tipless cantilevers (CSC37-No Al/tipless, Mikromash, nominal spring constant = 0.4 N/m) with an epoxy glue (JB-Weld, Sulphur Springs, TX, USA). Using a clean test grating (MikroMasch, Spain) reverse imaging of the attached colloids was conducted to determine the RMS roughness within the contact area and it was found to be less than 6.4 nm. Before starting the experiments, the tips were rinsed in an ethanol bath and cleaned by UV-O₃ (Bioforce Nanoscience, Chicago, IL) for half an hour. The normal stiffness of the cantilevers was determined by the thermal noise and the lateral calibration was performed following the modified Sader's method⁶⁷.

Microscale indentation was performed with the colloid on the cartilage sections at an approach/retraction velocity of 0.8 $\mu\text{m/s}$ at room temperature. Force maps were carried out on three different regions of the cartilage. Each force map consisted of 64 curves over an area of 10 x 10 μm . The Hertz model¹ was fit to the indentation curves upon extension of the colloid to the hydrogel:

$$F = \frac{4}{3} E^* R^{1/2} h^{3/2}$$

R being the radius of the colloid, h the indentation depth, and E^* the contact elastic modulus, i.e.

$$\frac{1}{E^*} = \left(\frac{1 - \nu_c^2}{E_c} \right) + \left(\frac{1 - \nu_{sil}^2}{E_{sil}} \right)$$

E_c being the elastic modulus of the cartilage, E_{sil} the elastic modulus of the silica colloid (72.2 GPa⁶⁸), and ν the Poisson's ratio of the cartilage ($\nu_c = 0.45$)⁶⁹ and silica colloid ($\nu_{sil} = 0.168$), respectively. As recently reported for hydrogels³⁶, this method estimates the change of the elastic modulus as a function of indentation depth, and thereby, allows the characterization of the graded microstructure of the cartilage sections from the top to the bottom. Under all conditions, the ratios a/R (a is the contact radius, $a = \sqrt{R \cdot d}$) and d/h are less than 0.3 and 0.1, respectively, indicating small deformations and no substrate effects⁷⁰, and hence justifying the use of the Hertz model to determine the elastic modulus.

Lateral force measurements were conducted at a lateral velocity of the piezo of 1 $\mu\text{m/s}$ at a constant scan length of 28 μm , and at three loads, 20, 30 and 50 nN at room temperature. The experiments were repeated at least on two different regions of the cartilage sections to confirm the reproducibility of the results. At the point of reversal of the piezo (i.e. under zero tangential force), the normal load was maintained constant for a period of time (t_{hold}) that ranged from 5 to 60 seconds; this was repeated three times per loading time. Both height and lateral deflection of the cantilever were inspected to ensure that pile-up did not happen³⁶.

The combination of experimental techniques, AFM imaging, nanoindentation and eSFA, provides complementary information of the structure of the cartilage's superficial zone at different length scales (Table S3). The sharp tip in QI imaging can resolve the microstructure of the cartilage with sub-micron resolution. Indentation depths smaller than 1 μm are achieved by AFM indentation with contact radius of less than 3.4 μm , whereas the contact radius probed by eSFA goes up to $\sim 400 \mu\text{m}$. For a poroelastic and viscoelastic material like cartilage, the time-dependent response to mechanical loading is also relevant: nanoindentation involves time scales smaller than 1.2 seconds, while the unconfined compression in eSFA experiments prolongs over several hours. Therefore, each experimental method probes significantly different length and time scales.

Conflicts of interest

There are no conflicts to declare.

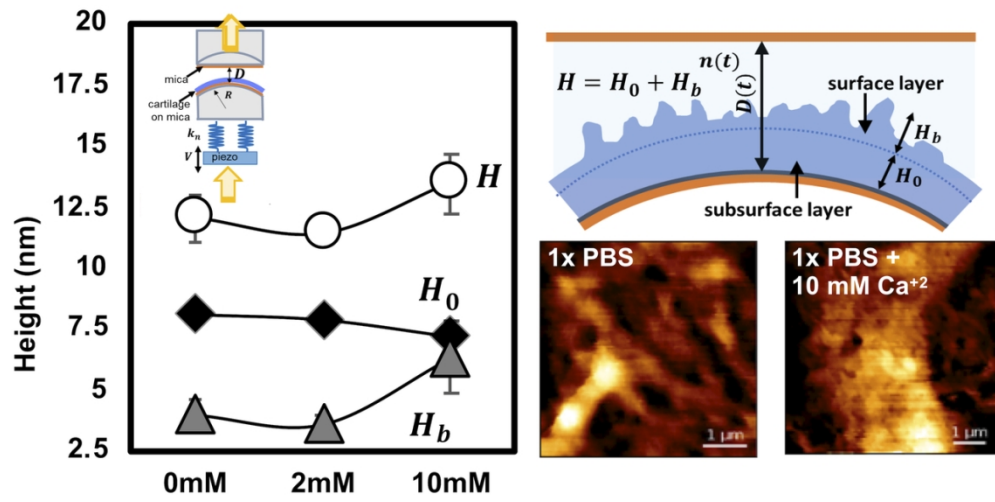
Acknowledgements

This work is supported by the National Science Foundation Grant No. 17-61696.

References

- H. Hertz, *Reine Angewandte Mathematik*, 1881, **92**, 156-171.
- J. A. Buckwalter, H. J. Mankin and A. J. Grodzinsky, *Instr Course Lect*, 2005, **54**, 465-480.
- S. Kobayashi, S. Yonekubo and Y. Kurogouchi, *J Anat*, 1996, **188 (Pt 2)**, 311-322.
- R. Teshima, T. Otsuka, N. Takasu, N. Yamagata and K. Yamamoto, *J Bone Joint Surg Br*, 1995, **77b**, 460-464.
- R. Crockett, S. Roos, P. Rossbach, C. Dora, W. Born and H. Troxler, *Tribol Lett*, 2005, **19**, 311-317.
- S. Jahn, J. Seror and J. Klein, *Annu Rev Biomed Eng*, 2016, **18**, 235-258.
- R. Boyanich, T. Becker, F. Chen, T. B. Kirk, G. Allison and J. P. Wu, *J Microsc*, 2019, **275**, 159-171.
- J. Yu and J. P. Urban, *J Anat*, 2010, **216**, 533-541.
- M. W. Ropes, G. A. Bennett and W. Bauer, *Journal of Clinical Investigation*, 1939, **18**, 351-372.
- G. W. Greene, R. Thapa, S. A. Holt, X. Wang, C. J. Garvey and R. F. Tabor, *Langmuir*, 2017, **33**, 2559-2570.
- J. Shao, L. Lin, B. Tang and C. Du, *RSC Adv.*, 2014, **4**, 51165-51170.
- Y. K. Jung, M. S. Han, H. R. Park, E. J. Lee, J. A. Jang, G. W. Kim, S. Y. Lee, D. Moon and S. Han, *Scientific Reports*, 2018, **8**.
- A. Mobasheril, C. Matta, I. Uzielienè, E. Budd, P. Martín-Vasallo and E. Bernotiene, *Joint Bone Spine*, 2019, **86**, 29-35.
- G. M. McCarthy and A. Dunne, *Nat Rev Rheumatol*, 2018, **14**, 592-602.
- L. G. E. Cox, B. van Rietbergen, C. C. van Donkelaar and K. Ito, 2011.
- S. H. Rhee, J. D. Lee and J. Tanaka, *Journal of the American Ceramic Society*, 2000, **83**, 2890-2892.
- A. Harder, V. Walhorn, T. Dierks, X. Fernandez-Busquets and D. Anselmetti, *Biophys J*, 2010, **99**, 3498-3504.
- W. T. Winter and S. Arnott, *J Mol Biol*, 1977, **117**, 761-784.
- H. Chen, M. Deere, J. T. Hecht and J. Lawler, *J Biol Chem*, 2000, **275**, 26538-26544.
- X. Pang, P. Sun, Z. Tan, L. Lin and B. Tang, *Materials Letters*, 2016, **180**, 332-335.
- F.-Z. Cui, Y. Li and J. Ge, *Materials Science and Engineering: R: Reports*, 2007, **57**, 1-27.
- S. J. Prestrelski, N. Tedeschi, T. Arakawa and J. F. Carpenter, *Biophys J*, 1993, **65**, 661-671.
- A. Mobasheril, R. Mobasheril, M. Francis, E. Trujillo, D. A. De La Rosa and P. Martin-Vasallo, *Histol Histopathol*, 1998, **13**, 893-910.
- A. Maroudas, in *The joints and synovial fluid*, Elsevier, 1980, pp. 239-291.
- T. E. Hargest, C. V. Gay, H. Schraer and A. Wasserman, *Journal of Histochemistry & Cytochemistry*, 1985, **33**, 275-286.
- J. M. Mansour, *Kinesiology: the mechanics and pathomechanics of human movement*, 2003, **2**, 66-79.
- B. Zappone, N. J. Patil, M. Lombardo and G. Lombardo, *Plos One*, 2018, **13**, e0197779.
- M. Stolz, R. Gottardi, R. Raiteri, S. Miot, I. Martin, R. Imer, U. Stauffer, A. Raducanu, M. Duggelin, W. Baschong, A. U. Daniels, N. F. Friederich, A. Aszodi and U. Aebi, *Nat Nanotechnol*, 2009, **4**, 186-192.
- J. Mansfield, J. Yu, D. Attenburrow, J. Moger, U. Tirilapur, J. Urban, Z. Cui and P. Winlove, *J Anat*, 2009, **215**, 682-691.

30. C.-C. Chen, A. L. Boskey and L. C. Rosenberg, *Calcified tissue international*, 1984, **36**, 285-290.
31. A. Maroudas, J. Mizrahi, E. Benaim, R. Schneiderman and G. Grushko, in *Mechanics of Swelling*, Springer, 1992, pp. 487-512.
32. U. Raviv, J. Frey, R. Sak, P. Laurat, R. Tadmor and J. Klein, *Langmuir*, 2002, **18**, 7482-7495.
33. S. Z. Wang, Y. P. Huang, Q. Wang, Y. P. Zheng and Y. H. He, *Connect Tissue Res*, 2010, **51**, 36-47.
34. P. G. de Gennes, *Advances in Colloid and Interface Science*, 1987, **27**, 189-209.
35. R. C. Andresen Eguiluz, S. G. Cook, C. N. Brown, F. Wu, N. J. Pacifici, L. J. Bonassar and D. Gourdon, *Biomacromolecules*, 2015, **16**, 2884-2894.
36. T. Shoaib and R. M. Espinosa-Marzal, *ACS Appl Mater Interfaces*, 2019, **11**, 42722-42733.
37. L. P. Li, J. Soulhat, M. D. Buschmann and A. Shirazi-Adl, *Clinical Biomechanics*, 1999, **14**, 673-682.
38. N. Alcantar, J. Israelachvili and J. Boles, *Geochim Cosmochim Acta*, 2003, **67**, 1289-1304.
39. H. Yoshizawa and J. Israelachvili, *J Phys Chem-U S A*, 1993, **97**, 11300-11313.
40. R. K. Iler, *New York*, 1979, 30-62.
41. R. K. Iler, *Journal of Colloid and Interface Science*, 1975, **53**, 476-488.
42. L. Han, D. Dean, L. A. Daher, A. J. Grodzinsky and C. Ortiz, *Biophys J*, 2008, **95**, 4862-4870.
43. S. D. Allison, B. Chang, T. W. Randolph and J. F. Carpenter, *Archives of Biochemistry and Biophysics*, 1999, **365**, 289-298.
44. R. Crockett, A. Grubelnik, S. Roos, C. Dora, W. Born and H. Troxler, *J Biomed Mater Res A*, 2007, **82**, 958-964.
45. D. Peer, A. Florentin and R. Margalit, *Biochimica et Biophysica Acta (BBA)-Biomembranes*, 2003, **1612**, 76-82.
46. C. J. Bell, E. Ingham and J. Fisher, *Proc Inst Mech Eng H*, 2006, **220**, 23-31.
47. H. Forster and J. Fisher, *Proc Inst Mech Eng H*, 1996, **210**, 109-119.
48. A. Maroudas, *Biophys J*, 1968, **8**, 575-595.
49. C. T. Bussiere, G. M. Wright and M. E. DeMont, *Comp Biochem Physiol A Mol Integr Physiol*, 2006, **143**, 417-428.
50. C. M. Kielty and C. A. Shuttleworth, *FEBS Lett*, 1993, **336**, 323-326.
51. T. M. Schmid, J.-L. Su, K. M. Lindley, V. Soloveychik, L. Madsen, J. A. Block, K. E. Kuettner and B. L. Schumacher, in *The Many Faces of Osteoarthritis*, 2002, DOI: 10.1007/978-3-0348-8133-3_16, ch. Chapter 16, pp. 159-161.
52. B. L. Schumacher, J. A. Block, T. M. Schmid, M. B. Aydelotte and K. E. Kuettner, *Arch Biochem Biophys*, 1994, **311**, 144-152.
53. F. Horkay, P. J. Basser, D. J. Londono, A. M. Hecht and E. Geissler, *J Chem Phys*, 2009, **131**, 184902.
54. P.-G. De Gennes and P.-G. Gennes, *Scaling concepts in polymer physics*, Cornell university press, 1979.
55. D. W. Lee, X. Banquy and J. N. Israelachvili, *Proc Natl Acad Sci U S A*, 2013, **110**, E567-574.
56. D. W. Nitzan, *Cells Tissues Organs*, 2003, **174**, 6-16.
57. C. Y. Wen, C. B. Wu, B. Tang, T. Wang, C. H. Yan, W. W. Lu, H. Pan, Y. Hu and K. Y. Chiu, *Osteoarthr Cartilage*, 2012, **20**, 916-922.
58. A. C. Moore and D. L. Burris, *Osteoarthritis Cartilage*, 2015, **23**, 161-169.
59. A. E. Peters, E. J. Comerford, S. Macaulay, K. T. Bates and R. Akhtar, *J Mech Behav Biomed Mater*, 2017, **71**, 114-121.
60. E. D. Eanes, A. W. Hailer, R. J. Midura and V. C. Hascall, *Glycobiology*, 1992, **2**, 571-578.
61. J. N. Israelachvili and D. Tabor, *Proceedings of the Royal Society A: Mathematical, Physical and Engineering Sciences*, 1972, **331**, 19-38.
62. M. Heuberger, *Review of Scientific Instruments*, 2001, **72**, 1700-1707.
63. M. Heuberger, J. Vanicek and M. Zäch, *Review of Scientific Instruments*, 2001, **72**, 3556-3560.
64. H. H. Chao and D. F. Torchiana, *Journal of cardiac surgery*, 2003, **18**, 500-503.
65. M. Heuberger and T. E. Balmer, *Journal of Physics D: Applied Physics*, 2007, **40**, 7245.
66. J. N. Israelachvili, *Intermolecular and surface forces*, Academic press, 3rd edn., 2011.
67. R. J. Cannara, M. Eglin and R. W. Carpick, *Review of Scientific Instruments*, 2006, **77**, 053701.
68. W. Pabst and E. Gregorova, *Ceramics-Silikaty*, 2013, **57**, 167-184.
69. A. Thambyah, A. Nather and J. Goh, *Osteoarthritis Cartilage*, 2006, **14**, 580-588.
70. P. C. Nalam, N. N. Gosvami, M. A. Caporizzo, R. J. Composto and R. W. Carpick, *Soft Matter*, 2015, **11**, 8165-8178.



112x56mm (300 x 300 DPI)